CFD simulation plus uncertainty quantification of the mixing of two fluid with different density for the Cold-Leg Mixing Benchmark.

Y. RIVERA[1], J.L. MUÑOZ-COBO[1], C. BERNA[1], A. ESCRIVÁ[1], E. VELA[2].

[1] Universitat Politècnica de València, Institute for Energy Engineering, (Valencia), Spain
Camino de Vera, 14. yaridu@upv.es
[2] Consejo de Seguridad Nuclear, Subdirección de Ingeniería, Spain

Keywords: Computational fluid dynamics, uncertainty quantification, polynomial chaos expansion, cold-leg mixing, benchmark.

Abstract. This document describes the details of the simulations and uncertainty quantification of the Cold-Leg Mixing benchmark performed at the Institute for Energy Engineering (Polytechnic University of Valencia, Spain). The experiment, carried out by Texas A&M University, consists of the mixing of two water flows with different densities inside two tanks joined by a pipeline or cold leg. The tank that accumulates the low-density water and its connection to the cold leg are designed to create a downcomer like the one found in a PWR reactor vessel. On the other hand, the high-density water reservoir represents the cold-water injection accumulator. The method of Polynomial Chaos Expansion (PCE) based on Gaussian Quadrature is applied to calculate the uncertainty of the results, and a model created in Ansys CFX is developed to carry out the simulations. A 5^{th} order Polynomial Chaos Expansion by Gaussian-Hermite Quadrature has been applied using as uncertain parameter the density difference between the mixing fluids. Therefore, five simulations have been done for both the open and the blind test. This methodology aims to provide an efficient solution since PCE solved by Gaussian Quadrature allows to obtain uncertainty quantification through a low number of simulations when the amount of uncertain input variables is low. It has been observed that the turbulence model significantly affects the results obtained, being the LES model the only one able to reproduce the real behavior consistently. Simulation results show a good agreement with experimental data for the cold-leg measurement zone while, in the downcomer a slightly different velocity profile than the one measured experimentally is obtained. The concentration profile of each fluid shows a gap in the transition zone that does not seem to agree with the velocity results. That behavior remains for higher time averages when comparing simulation results with experimental measurements.

1 INTRODUCTION

Computational Fluid Dynamic (CFD) codes are a very useful tool in the nuclear field but there are still scenarios in which their application is complex or requires high computational power. To validate the results obtained with these codes it is necessary, among other things, to carry out studies based on experimental measurements (ASME V&V 20, 2009). A very good way to advance in the validation of CFD codes is to carry out benchmarks in which different

organizations or companies at an international level participate by simulating a concrete experiment using different CFD codes and different modeling approaches. This practice serves to share the different methodologies and codes used by the different participants, as well as to increase the know-how about the different CFD models, as for instance averaged Navier Stokes Equations with k-epsilon model or Large Eddy Simulation model (LES), when we apply this kind of codes to different types of experiments.

CFD codes are a widely used tool in the nuclear field because of the multiple applications, which they have both in design and licensing of nuclear power plants and in addition in nuclear reactor safety (Mahaffy et al., 2014). This type of methods is especially useful when we focus on studying the specific operation of a reactor component, being able to observe the behavior of the fluids moving inside of it. Despite being available for several years, CFD codes still require a lot of research to ensure that the results are correct; especially in scenarios where safety is the most relevant factor. However, best practice guidelines for the nuclear codes in nuclear safety applications developed in the last few years have increased the confidence of the regulatory bodies in this type of codes (Mahaffy et al., 2014). Nevertheless, CFD codes are becoming more and more established as they offer great advantages such as the possibility of simulating complex 3D geometries, optimized numerical codes, etc (Smith et al., 2008).

To continue making progress in the use and knowledge of CFD codes, the Institute of Energy Engineering of the Polytechnical University of Valencia (UPV) has participated with many organizations of different countries as PSI, CEA, NRC, JAERI, KAERI, among others. In the six latest benchmarks organized by the OECD/NEA WGAMA group, including:

- OECD/NEA-Vattenfall CFD Benchmark Exercise 2008-2010. Simulation of an experiment in one of the facilities of the Älvkarleby laboratory, Vattenfall Research and Development about mixing fluids at different temperatures in a T-junction. Details could be found in Smith et al. (2013) and the official OECD/NEA report (OECD/NEA/ CSNI et al., 2011).
- OECD/NEA-KAERI CFD Benchmark Exercise 2010-2012 Simulation of the MATiS-H experiment that studies the cross flow in a subchannel with several measurements downstream of a spacer grid. All the information can be found in the document presented by Chang et al. (2014) and in the OECD/NEA/CSNI report (B.L. Smith et al., 2013).
- OECD/NEA-PSI CFD Benchmark Exercise 2012-2014. Simulation of an experiment in the PANDA installation of the PSI about helium concentration in different parts of a vessel. A synthesis of the benchmark exercise is described in Andreani's et al. (2016) paper and a more detailed report can be found in OECD/NEA/CSNI (2016).
- OECD/NEA-PSI CFD Benchmark Exercise 2014-2016. Simulation of an experiment in the PSI GEMIX installation about the mixing of two fluids with different temperature. In this benchmark, in addition to the modeling, the participants were required to calculate the uncertainty of the simulations. The most important information and all the data can be found in the report Fokken et al. (2019) and the paper Badillo et al. (2013).

- OECD/NEA-Texas A&M University Benchmark Exercise 2017-2019 Simulation of an experiment in the COLD-LEG MIXING installation of Texas A&M University about the mixing of two fluids with different density ($\Delta\rho$ between $100 - 200\, kg/m^3$). Authors have already published a paper (Orea et al., 2020) explaining the experimental approach, measurement techniques, test conditions and results. Some of the more active members of the benchmark group are already writing the official OECD/NEA report and it is expected to be available soon.

In the field of nuclear reactor safety, it is mandatory to know the uncertainty of the predictions obtained from computational codes. These statistical techniques are known as Best Estimate plus Uncertainty (BEPU) methodologies because these codes use the best physical and numerical methods available (state of the art) and at the same time these methodologies include an estimation of the uncertainty in the results (D 'Auria et al., 2012). Therefore, different techniques are being adapted for their use in CFD simulations considering both intrusive and non-intrusive methodologies. For the last two benchmark exercises, GEMIX (Fokken et al., 2019) and Cold-leg mixing, the study has been extended to consider not only the development of the model but also the uncertainty quantification of the results.

This research together with that of the other participants will show the capabilities of CFD codes to predict fluid mixing by turbulence and buoyancy effects. The results obtained by the Institute for Energy Engineering and the different international organizations that are involved in these benchmarks will be used to develop a set of best practices guidelines (also known as BPG) for the use of CFD codes for Nuclear Reactor Safety issues. As a reference, the document (Mahaffy et al., 2014) collect a lot of information regarding this aspect, but more documentation can be added to a new version for both new and experienced users.

Throughout this paper, the application of CFD methods to the scenario selected for the Cold Leg Mixing benchmark exercise is shown. As usual in these activities, the exercise consists of two assessment, first an open test from which the experimental measurements are known, and secondly a blind test from which only the initial conditions are given to the participants. For each of those tests two different parts have been addressed throughout the document. Firstly, the development of the experimental facility model which includes the activities of geometry generation, mesh development and optimization, preparation of the setup and the different simulation models, and post-processing. The second step is the development of an efficient methodology of uncertainty quantification for the predictions of the model of the experimental facility. For this purpose, the different alternatives already known by other authors must be studied and the most convenient one selected. For this benchmark it has been decided to use the Polynomial Chaos Expansion (PCE) based on Gaussian Quadrature because of its efficiency when the number of uncertain variables is small.

The theoretical aspects of PCE were first developed by Wiener (1938), and later generalized by Xiu and Karniadakis (2003a), based on previous studies by Askey and Wilson (1985). Since the early stages of its development, PCE has been successfully applied to numerous CFD simulations, and more recently to system thermal-hydraulic codes by Muñoz-Cobo et al. (2018).

A complete review of the different PCE techniques, along with some CFD applications, is presented by Knio and Le Maître (2006) and Najm (2009).

Special mention should be made of the study carried out in Badillo's et al. (2013) research where the PCE method is applied to quantify the uncertainty in the GEMIX Benchmark results. The authors used a methodology similar to the one presented in this paper although they chose Collocation Points instead of Gaussian Quadrature as the technique for the resolution of the system derived from the Polynomial Chaos Expansion.

Many investigations have emerged from GEMIX benchmark, proposing different uncertainty quantification methodologies. For example in Rakhimov's et al. (2018) research the Latin Hypercube Sampling (LHS) technique is applied following the ASME standard for verification and validation in CFD and Heat Transfer (ASME V&V 20, 2009) obtaining a good agreement between experiment and simulation. Moreover, the authors present in Rakhimov et al. (2019) the application of the Deterministic Sampling (DS) technique based on the research done by Hessling (2013) to increase the efficiency by reducing the number of simulations required while maintaining a high level of reliability. In addition, they carry out comparisons between DS-standard ensemble and DS-simplex ensemble, obtaining the highest degree of accuracy-efficiency with the second one.

A different approach is investigated in the paper presented by Prošek et al. (2017), where the authors use the Optimal Statistical Estimator (OSE) method as response surface generator to apply in Monte Carlo analysis. This method, as the one presented in this paper, is optimal when the number of uncertain variables is small. Consequently, they need a total of 30 simulations when two input parameters are considered as uncertain variables.

Many other authors have presented interesting results on the GEMIX benchmark although some of them without uncertainty calculation as Krpan and Končar (2018) or Kim (2019). This paper aims to bring the Polynomial Chaos Expansion by Gaussian Quadrature methodology for the calculation of uncertainty in CFD simulations to all, allowing its application in an efficient way. Therefore, it is possible to overcome the high computational cost barrier derived from the use of CFD in simulations where the uncertainty calculation is needed.

In order to achieve the objectives mentioned in this introduction, the document is structured as follows. Section 2 contains the information related to the experimental installation. The section 3 covers the details of the model and the simulation conditions, and the section 4 the quantification of the uncertainty. Finally, section 5 contains the results obtained and their discussion, followed by the conclusions of the research.

2 EXPERIMENTAL FACILITY COLD-LEG MIXING

The Cold-Leg Mixing Texas A&M University experiment (Orea et al., 2020) adds some complexity to the previous GEMIX benchmark (Badillo et al., 2013) performed at PSI. The geometry becomes more realistic in relation to the design of a light water PWR and the

phenomena involved are transient. Following the guidelines of the previous benchmark, participants should carry out an uncertainty calculation (UQ) under conditions, which are closer to the existing ones in real reactors.

The experiment consists of two streams of water of different densities that are mixed after the opening of a valve located approximately in the center of a pipeline that links two liquid tanks (Figure 1a). The left tank contains the high-density fluid, and the right tank contains the lighter fluid as happens inside the downcomer of the reactor vessel. The two fluids are initially at rest and when the valve is opened, a temporary mixing process of several minutes begins, because of the heavier fluid tends to move below the lighter one towards the downcomer.

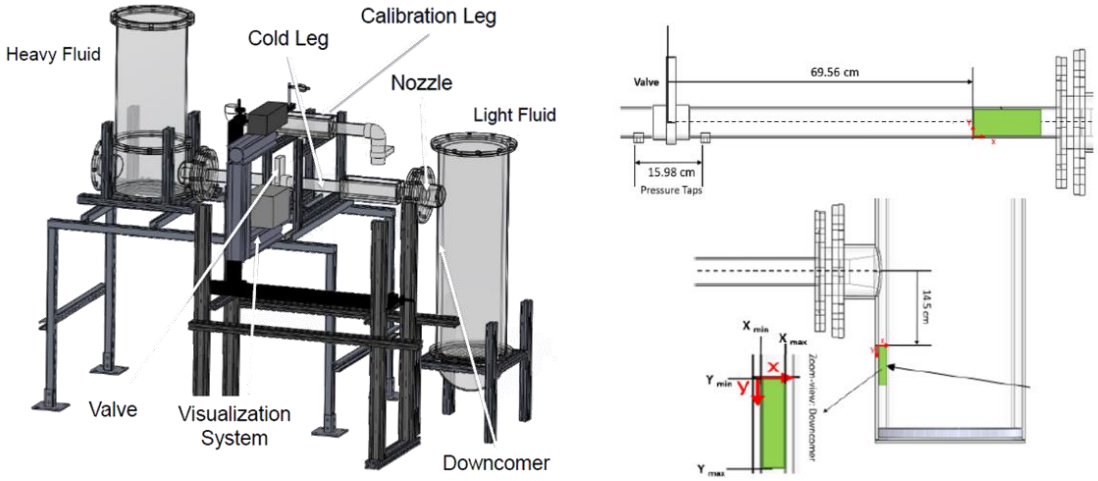

Figure 1: Experimental facility Cold-Leg Mixing (Orea et al., 2020) (a) 3D design and (b) Measurement zones of the experiment: Cold-Leg on the upper side (PIV+LIF) and below the downcomer zone (PIV).

Texas A&M University carried out velocity measurements in two study areas (Figure 1b) using a PIV (Particle Image Velocimetry) system. The first zone is located near the end of the cold-leg, and the second one in the entrance zone to the downcomer. In the first zone, in addition to the PIV system, the density has been measured using a LIF system (Laser-induced fluorescence). Detailed information about the experiment can be found in (Orea et al., 2020).

The characteristics of the fluids for the open test are shown in Table 1. Additionally, the standard deviations of the measurements of the properties of the two fluids denoted as $\sigma_H \; and \; \sigma_L$are 6.505 and 7.311 kg/m^3 respectively and the viscosity $\pm 1.5\%$ for both fluids. The Atwood number is defined as the ratio of the difference of the densities divided by their sum.

Table 1. Fluid characteristics for the open and blind test.

Case	Fluid	Density $[kg/m^3]$	Density difference $[kg/m^3]$	Atwood Number	Viscosity $[Pa \cdot s]$
OPEN TEST	High density	1064.7	108.16	0.054	$1.09 \cdot 10^{-3}$
	Low density	956.54			$2.45 \cdot 10^{-3}$
BLIND TEST	High density	1107.07	195.73	0.097	$1.377 \cdot 10^{-3}$
	Low density	911.34			$2.847 \cdot 10^{-3}$

Three Reynolds numbers have been obtained for near-developed conditions, two in the cold-leg and one in the downcomer. Since in the cold-leg the two fluids move in different directions, an approximate hydraulic diameter has been obtained taking into account the position of the interface between both fluids. In the downcomer, the downward movement of the mixture predominates, so only one Reynolds number has been calculated. Table 2 shows their values for both the Open Test and the Blind Test. Fluids moving along the cold-leg have a Reynolds number much lower than that of the downcomer mixture. This is directly related to the flow regime and turbulence of each of these zones. In the cold-leg, buoyancy and gravity forces predominate although eddies can be seen at the front of the moving fluid. With time, slight oscillations also appear at the interface. On the other hand, in the downcomer, turbulence predominates over other forces

Table 2. Characteristic velocities, lengths and Reynolds Numbers for the Open and Blind Test.

OPEN TEST				
Zone	Fluid	Characteristic velocity [m/s]	Characteristic length [m]	Reynolds Number
Cold-Leg	Low-density fluid	0.054	0.038	2060
	High-density fluid	0.075	0.026	1964
Downcomer	Mixture	0.194	0.078	15137
BLIND TEST				
Zone	Fluid	Characteristic velocity [m/s]	Characteristic length [m]	Reynolds Number
Cold-Leg	Low-density fluid	0.067	0.038	2527
	High-density fluid	0.116	0.027	3114
Downcomer	Mixture	0.212	0.078	16497

To focus the experiment only on the phenomenology derived from the density difference between the fluids, the heights of the low-density water and high-density water tanks were balanced so that the pressure difference on both sides of the valve located in the pipe center was equal to zero. Thus, for the open test, the high-density liquid tank reached the height of

25.06 cm while for the blind test only 22.97 cm were needed. This must be considered since it is needed to vary the geometry and the mesh depending on the test that we want to perform.

The experiment starts with the opening of the valve. At this moment, the two fluids, which had remained separated, begin to mix. The high-density fluid starts to flow through the bottom of the pipe entering the region where there was only low-density fluid (first measurement area). At some point, the high-density fluid reaches the low-density liquid tank and descends through the downcomer, thus reaching the second measurement zone. The opening of the valve has been simplified, so the start of the simulation is the opening of the "invisible wall" that separates the high and low density fluid instead of the physical opening of a valve. The total measurement time is 42 seconds.

Benchmark participants must simulate this behavior of the fluid by means of CFD codes. In addition, they need to carry out an uncertainty study of the most important output variables. Table 3 shows the required averages in 2 lines located in the cold-leg and another 2 in the downcomer. Note that the prefix “d” refers to the uncertainty or error, e.g. U-dU would correspond to the mean value of U minus the lower error band.

Table 3. Averaged variables required for the Cold-Leg Mixing benchmark and its averaged upper and lower uncertainty band.

Name	**Variables**	**Equation**
Mean velocity components	U, U-dU, U+dU, V, V-dV, V+dV [cm/s]	$U_{mean} = U = \frac{1}{N}\sum_{i=1}^{N} u_i$
Standard deviation of the velocity components	U_{sd}, U_{sd}-dU_{sd}, U_{sd}+dU_{sd}, V_{sd}, V_{sd}-dV_{sd}, V_{sd}+dV_{sd} [cm/s]	$U_{sd} = \sqrt{\frac{1}{N-1}\sum_{i=1}^{N}(u_i - U_{mean})^2}$
Reynolds stresses	Re_{stress}, Re_{stress}-dRe_{stress}, Re_{stress}+dRe_{stress} [cm^2/s^2]	$Re_{stress} = \frac{1}{N-1}\sum_{i=1}^{N}(u_i - U_{mean})(v_i - V_{mean})$
Concentration (only in the cold-leg)	C, C-dC, C+dC [%]	$C_{mean} = C = \frac{1}{N}\sum_{i=1}^{N} c_i$

The averaged times intervals of the velocity are 0-5s, 5-10s, 10-15s, 15-22.5s, 0-10s y 10-22.5s in the cold-leg. In the downcomer the averages are 10.5-15.5s, 15.5-20.5s, 20.5-25.5s, 25.5-30.5s, 30.5-35.5s, 35.5-41.538s, 10.5-20.5s, 20.5-30.5s, and 30.5-41.538s. Therefore, each participant must provide all the averages defined in Table 3 for each variable.

In addition, to this set of averaged measures, it is also necessary to present measures of instantaneous variables, see Table 4. The timestep used is a decision of each participant. As for the averaged variables, its two error bands should be send along with each instantaneous result.

Table 4. Instantaneous variables required for the Cold-Leg Mixing benchmark.

Name	Variables	Details
Instantaneous velocity	u_i, u_i-du_i, $u_{i+}du_i$ v_i, v_i-dv_i, $v_{i+}dv_i$	Speed u_i and v_i in 6 determined points of the cold leg from the second 0 to 22.24 and other 6 points of the downcomer between the seconds 10.5 and 41.538.
Instantaneous concentration (only in the cold leg)	c_i, c_i-dc_i, $c_{i+}dc_i$	Instantaneous concentration in the 6 points of the cold leg from the second 0 to 22.24 and their corresponding error bands.

3 CFD MODEL

The CFD code Ansys CFX has been used to make the model. The geometry of the experimental setup provided by Texas A&M University is shown in Figure 2. The part of the domain where the low-density fluid is stored is represented by the blue color. On the other side, the orange color corresponds to the high-density fluid. In the middle of the pipe is located the valve, which starts the experiment after opening allowing the motion and the mixing of both fluids. Adjustments has been implemented in the geometry provided by TAMU to decrease the incompatibility problems with the Ansys geometry manager. For this purpose, a debugging and reduction of sharp edges has been carried out.

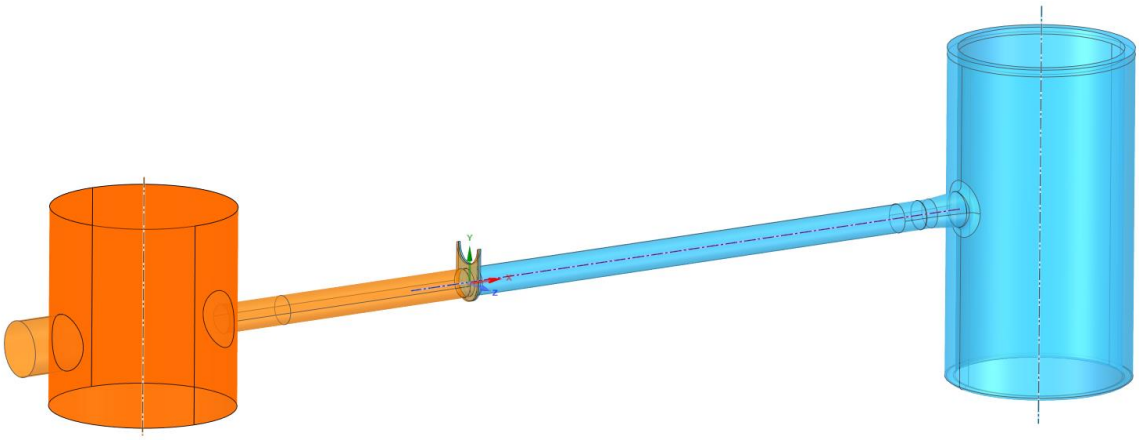

Figure 2: Domain geometry provided by (Orea et al., 2020).

ICEM CFD software has been selected to create the unstructured, conformal hexa mesh. Figure 3 shows the details of some important parts of the mesh. The total number of nodes of the mesh is 4 million.

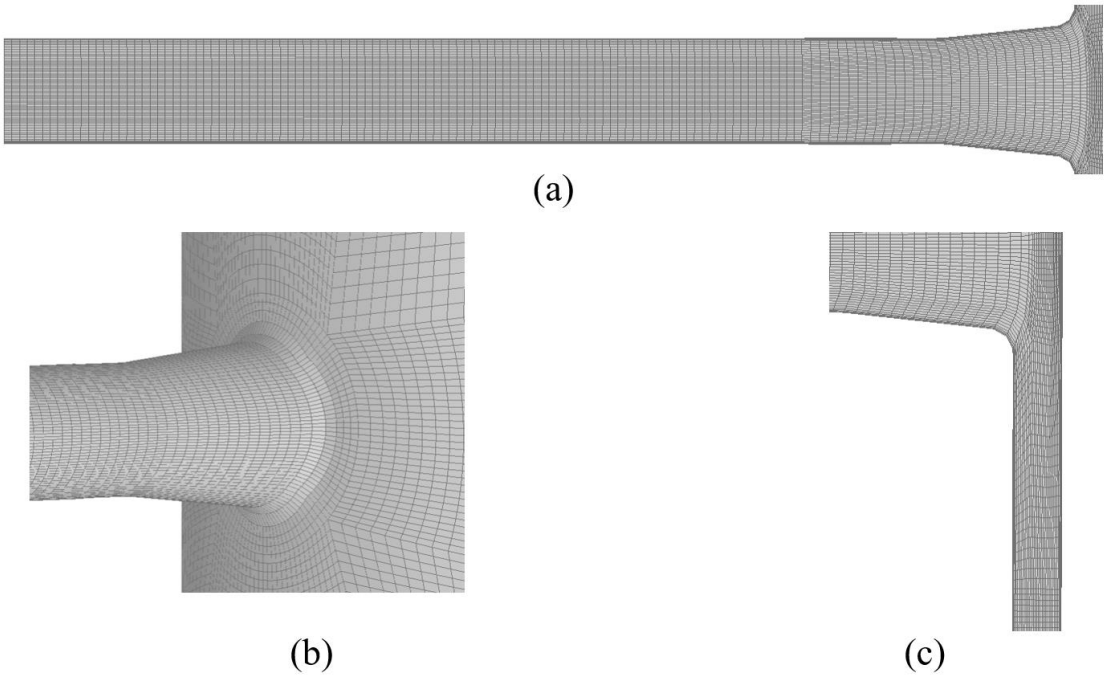

Figure 3: Mesh details, (a) longitudinal cut of the cold leg, (b) connection between the cold leg and the downcomer and (c) longitudinal cut of the cold leg and downcomer connection

In order to facilitate the replicability of the simulations Table 5 has been included, showing the most important parameters and models used in the simulations. The column corresponding to the LES model represents the final configuration used for the benchmark simulations, as well as for the simulations performed for uncertainty quantification.

Table 5. Most important model and parameters applied for the different simulations.

	LES SIMULATION	DES	SST	LAMINAR
Code	CFX	CFX	CFX	CFX
Fluid modelling approach	LES SIMULATION	Hybrid	URANS	LAMINAR
Specific turbulence (URANS) or SGS (LES) model	Smagorinsky	Detached eddy simulation	SST	-
Variable density treatment	Density difference			
Advection Scheme	Central Difference Scheme	CFX High resolution scheme	CFX High resolution scheme	CFX High resolution scheme

Time discretization scheme	Second order backward Euler			
Time step size (dt)	0.005s			
Total time	42s	20s	60s	60s
Maximum and average CFL	13 (max)	8 (max)	7 (max)	10 (max)
	0.4 (average)	0.23 (average)	0.2 (average)	0.34 (average)
Meshing features	4 million nodes, unstructured, conformal, hexa mesh	2 million nodes, unstructured, conformal, hexa mesh	1.5 million nodes, unstructured, conformal, hexa+tetra	1.3 million nodes, unstructured, conformal, hexa
Wall treatment - type possibly including details on near wall damping	Automatic CFX near-wall treatment	Automatic CFX near-wall treatment	Automatic CFX near-wall treatment	-
Wall treatment - maximum y+ value	30 (max)	25 (max)	23 (max)	-
	1.3 (ave)	1.7 (average)	0.7 (average)	-
Boundary condition for the free surface	No-slip wall			
Modelling/assumptions for the valve opening	Opening not modelled. Fluid domain initialized at heavy fluid mass fraction equal 1 and 0 on the heavy and light side, respectively.			

Following the parameters included in CFD best practice guidelines (Mahaffy et al., 2014) and Ansys Meshing User Manual (Canonsburg, 2011), almost all of the mesh elements are within the high quality rating. There are certain regions of the mesh that are outside the best quality parameters. These zones are very complicated to mesh keeping the different parameters of quality of mesh at a high value. Each one of the most compromised elements has been analyzed and it has been observed that its impact in the solution is very small.

Figure 4 shows the elements that remains outside the high-quality standards. As can be seen, these elements are mainly found in the high-density water tank and do not pose a problem for the motion of the fluid in this experiment. Most of the volumes could be eliminated by increasing the refining of the mesh, but the computational cost is too high to justify it (Salvetti et al., 2018).

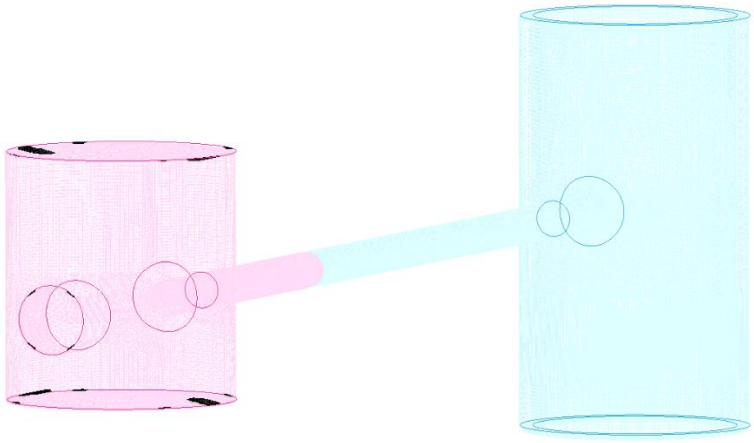

Figure 4: Lower quality elements of the mesh located entirely in the upper and lower area of the high-density water tank

The total simulation time was 42 seconds in order to measure the high-density fluid flowing down the downcomer. The timestep was set to 5 milliseconds in order to obtain acceptable Courant numbers during the transient simulation. The time scheme used in all cases is Second Order Backward Euler, which is an implicit time-stepping scheme with a second order accuracy in the time derivative. All the boundaries correspond to walls so there are no inlets or outlets and the velocity was fixed at 0 using the No Slip Wall model. Table 5 also shows the maximum and average y+ value for each of the simulations. It is important to mention that CFX includes a special wall treatment that automatically switches between wall functions and low-Re approach depending on the spacing in the wall zone. A homogeneous model has been adjusted for both phases and for the temperature transfer (at 22.5 ºC).

In many scenarios the Large Eddy Simulation (LES) turbulence model is the most realistic and most reliable model for simulating turbulence (Simoneau et al., 2010). However, the high cost in terms of computational time limits the application capabilities of many uncertainty quantification techniques that require performing many simulations. For this reason, before selecting the turbulence model to be used, several tests were performed with different models including: Laminar, Shear Stress Transport (SST), Detached Eddy Simulation (DES) and Large Eddy Simulation (LES) among others. It should be mentioned that the model that best reproduced the behavior of the experiment was the LES model in its three variations of sub-grid eddy models Smagorinsky, WALE and Dynamic Model. Further information about the results of each turbulence model is shown in section 5.

Between the two options of buoyancy model that CFX has implemented, density difference and Boussinesq, the first one usually offers slightly better results than the second one. The savings in computational time are practically negligible in this second option so the Density Difference model was used for most of the simulations. Central difference scheme was used for the LES simulations.

The final mesh size decision was made according to a sensitivity study and the available computational capacity. Table 6 shows some of the most important parameters of the meshes used in the sensitivity analysis. The study was performed with the LES Smagorinsky turbulence model during 20s and the only parameter that was modified was the number of nodes. Thus, three grids were defined (coarse, medium and fine) with approximately 1, 4 and 8 million nodes respectively.

Table 6. Mesh sensibility study parameters.

Parameter	Coarse	Medium	Fine
Total number of nodes	1 million	4 million	8 million
Turbulence model	LES Smagorinsky		
Max/mean y+	35 (max)	30 (max)	28 (max)
	3.3 (average)	1.3 (average)	1.1 (average)
Max/mean Courant Number	3 (max)	14 (max)	10 (max)
	0.1 (average)	0.34 (average)	0.1 (average)
Max Mesh Expansion Factor and percentaje of elements from 20 to max	53	30	26
	0.5% from 20 to 53	0.2% from 20 to 30	0.07% from 20 to 26
Max Aspect Ratio and percentaje of elements from 30 to max	64	50	55
	4.7% from 30 to 64	4.4% from 30-50	0.1% from 30 to 55
Min equiangle skewness and percentaje from min to 0.5	0.17	0.2	0.25
	3.9% from 0.17 to 0.5	3.5% from 0.2 to 0.5	4.2% from 0.25 to 0.5
Timestep	5 ms		
Type of mesh	Unstruc. hexa		

The difference between the meshes was evaluated in two areas (cold-leg and downcomer), following the measurement zones of the experiment. Table 7 shows the values of maximum velocity, average velocity and maximum density obtained for these reference zones. Additionally, two columns are included with the percentage variation of these variables between grids. It can be seen that in the case of velocities and densities in the cold leg, the values are much tighter. However, in the downcomer the difference is much more appreciable. Although the behavior of these variables was analyzed for the different meshes, the high computational cost greatly limited the possibilities of performing the simulations with a fine mesh. Since the main objective was to develop and test the uncertainty quantification methodology using polynomial chaos, it was necessary not only to carry out the different initial studies but also the different simulations for the calculation of the error bands. Consequently,

the 4 million mesh was selected. The mesh behaved quite well in the cold-leg although larger discrepancies were expected in the downcomer.

Table 7. Sensibility study results for coarse, medium and fine meshes.

		Coarse	Medium	Fine	Percentage of difference	
					From Coarse to Medium	From Medium to Fine
Cold-Leg	Max velocity	0.039	0.105	0.099	63%	6%
	Mean Velocity	0.0051	0.0106	0.0091	52%	16%
	Max density	1008	1048	1047	4%	1%
Downcomer	Max velocity	0.19	0.256	0.33	26%	22%
	Mean Velocity	0.182	0.235	0.278	23%	15%
	Max density	981	988	993	1%	1%

4 UNCERTAINTY QUANTIFICATION

Two models of uncertainty quantification have been considered for this benchmark. Firstly, Wilks method is reliable and easy to implement but has the important drawback of requiring almost 100 simulations to meet the usual safety requirements of coverage and confidence. This methodology can become very expensive in terms of computational cost if the simulations are time-consuming. On the other hand, Polynomial Chaos Expansion method (also known as PCE) is a more efficient alternative when the number of uncertain variables is small. For this reason, Polynomial Chaos Expansion method has been selected for the uncertainty quantification. In this benchmark there is a variable whose uncertainty is very relevant in the simulation results: the density. To avoid a very pronounced increase in simulations, the less relevant uncertain variables have been discarded because of their low impact on the results, for example, viscosity. Future analyses will also take into account subscale constants as they may affect the results depending on the importance of small scales in this type of simulations (Lucor et al., 2007).

$$\Delta\rho = \rho_H - \rho_L \tag{1}$$

$$\sigma_{\Delta\rho} = \sqrt{{\sigma_H}^2 + {\sigma_l}^2} \tag{2}$$

Being $\Delta\rho$ the density difference between heavy (ρ_H) and light (ρ_L) fluids and $\sigma_{\Delta\rho}$ its standard deviation. The uncertainty of the density difference between fluids follows a Gaussian probability distribution so Hermite polynomials were used (Wiener, 1938).

In PCE the response of a system $R(x)$, which depends on a set of uncertain parameters x, is expressed as a linear combination of a certain orthogonal basis of orthogonal polynomials $\{\phi_i\}_{i=0}^{\infty}$ known as Askey polynomials. The type of these polynomials depends on the probability distribution functions (PDF) of the uncertain parameters (Xiu and Karniadakis, 2003a):

$$R(x) = \sum_{n=0}^{\infty} \alpha_n \phi_n(x) \tag{3}$$

The parameters x $(x_1, x_2, \dots, x_{n_u})$ are usually assumed to be statistically independent, and therefore the PDF is written as $p(x) = \Pi_{i=0}^{n_u} p_i(x_i)$. Then, based on the orthogonal property of these polynomials the expansion coefficients α_i in eq. (3) are given by:

$$\alpha_n = \frac{1}{\langle {\phi_n}^2 \rangle} \int_X p(x)\, R(x) \phi_n(x)\, dx \tag{4}$$

Being

$$\langle {\phi_n}^2 \rangle = \int_X p(x)\, {\phi_n}^2(x) dx \tag{5}$$

The mean μ_R and the variance σ_R^2 of the system response $R(x)$, can be obtained easily from (3) using the orthogonality condition of the base functions and choosing without loss of generality $\phi_0 = 1$. Then, the mean is obtained computing the expected value of eq. (3), which yields:

$$\mu = \langle R(x) \rangle = \alpha_0 \tag{6}$$

While the variance is obtained from the variance definition on account of eq. (6), and the orthogonality condition of the base functions:

$$\sigma_R^2 = \langle R(x) - \mu^2 \rangle = \sum_{n=1}^{\infty} {\alpha_n}^2 \langle {\phi_n}^2 \rangle \cong \sum_{n=1}^{N} {\alpha_n}^2 \langle {\phi_n}^2 \rangle \tag{7}$$

The first simplification used to compute the variance was to reduce the number of terms in the expansion to a finite number N as displayed in equation (7), the value chosen for N is discussed later. It is important to highlight that the number of terms in the PCE of the system response is $N + 1$, because there is a term that contains α_0. First, we notice that because of the PDFs of the uncertain parameter is the fluid density and this density follows according to the test specifications a Gaussian distribution function, then it follows that the orthogonal polynomials must be the Hermite ones denoted by $H_n(x)$, being n the order of the polynomial. Then, the Gauss-Hermite quadrature method with 5-th order Hermite polynomials is applied, which is valid for any function $f(x)$, to compute the integrals of equations (4) and (5):

$$\int_{-\infty}^{\infty} e^{-x^2} f(x)\, dx = \sum_{j=1}^{m=5} w_j\, f(x_j) \tag{8}$$

Being w_j the quadrature weights and x_j the zeros of the Hermite polynomials used in defining the quadrature order $n_q$in this case 5. We remind that the Gauss-Hermite quadrature method of integration it is exact when $f(x)$ is a polynomial of degree $2n_q - 1 = 9$.

Because of the PDF of the input uncertain variable of this benchmark (density difference between fluids) x^{in} follows a Gaussian distribution with mean μ and standard deviation σ, then the integrals that are necessary to compute the coefficients α_n of the expansion can be written as follows. Note that eq. 9 and 10 are calculated in Appendix A, where we show the reasoning followed to obtain the integrals whose polynomials are orthogonal after the variable change (to fit the mean and variance of our uncertain variable).

$$\begin{aligned}\langle R\phi_n\rangle &= \int_{-\infty}^{\infty} \frac{1}{\sqrt{2\pi}\sigma} e^{-\left(\frac{x^{in}-\mu}{\sqrt{2}\,\sigma}\right)^2} R\left(x^{in}\right) He_n^{(\sigma^2,\mu)}\left(x^{in}\right) dx \\ &= \frac{\sigma^n}{\sqrt{\pi}\, 2^{n/2}} \sum_{j=1}^{5} w_j\, R\left(\mu + \sqrt{2}\,\sigma\, x_j\right) H_n\left(x_j\right)\end{aligned} \tag{9}$$

And

$$\langle {\phi_n}^2\rangle = \langle \left(He_n^{(\sigma^2,\mu)}\right)^2\rangle = \int_{-\infty}^{\infty} \frac{1}{\sqrt{2\pi}\sigma} e^{-\left(\frac{x-\mu}{\sqrt{2}\,\sigma}\right)^2} \left(He_n^{(\sigma^2,\mu)}(x)\right)^2 dx = \sigma^{2n}\, n! \tag{10}$$

Being $He_n^{(\sigma^2,\mu)}\left(x^{in}\right)$ the Hermite polynomial, which are orthogonal with the weight function $N(\mu,\sigma)$. The variable change of equation (11) was performed in the input uncertain variable, in order to use the standard Hermite quadrature method (Abramovitz and Stegun, 1972). Notice that to perform the calculations with the CFD code we must input to the code the set of input values$\left\{x_j^{in}\right\}_{j=1}^{5}$, given by the expression:

$$x_j^{in} = \mu + \sqrt{2} \cdot \sigma \cdot x_j \tag{11}$$

Being x_j the roots of the Hermite polynomials of 5-th order and x_j^{in}, the input values of the uncertain parameter that must be supplied to the CFD code in order to obtain the code response.

A polynomial expansion of order 4 has been selected to quantify the uncertainty by means of Polynomial Chaos in the Cold-Leg Mixing benchmark, although other authors claim that using polynomials of order 2 achieves a fairly good precision (Safta *et al.*, 2017). The number of terms of the expansion $N + 1$ and the minimum number of simulations points n_{sim} needed to achieve a good accuracy when we have n_u uncertain input parameters, and we perform the Hermite-Gauss quadrature integration with n_q weights and the PCE up to order q, is given by equation (12) and (13) as reported in (Xiu and Karniadakis, 2003b), (Richard. Askey and Wilson, 1985) and (Crestaux et al., 2009).

$$N + 1 = \frac{(n_u + q)!}{n_u!\, q!} \tag{12}$$

$$n_{sim} = n_q^{n_u} \tag{13}$$

Therefore, for this benchmark we have performed the integrals in (9) by means of Gauss-Hermite quadrature of 5th order (five zeros and weights per dimension). In this case, the number of uncertain parameters is only one, so the number of simulations needed is five and the number of terms of the Polynomial chaos expansion is also five. Table 8 displays the weights and the roots when using Gauss-Hermite quadrature.

Table 8. Roots of the 5th order Hermite Polynomials and its correspondent density value.

Roots x_j	-2.0202	-0.9586	0	0.9586	2.0202
Weights w_j	0.001993	0.393619	0.945308	0.393619	0.001993
OPEN TEST $\Delta\rho\ x_j^{in}$	80.2	94.9	108.2	121.4	136.1
BLIND TEST $\Delta\rho\ x_j^{in}$	167.7	182.4	195.7	208.9	223.6

To achieve a better understanding on the procedure performed to calculate the uncertainty of the results, the steps carried out are shown below:

1. The Matlab® script first loads all the vectors R, obtained for each output variable. This R vector corresponds to each variable for which we wish to know the uncertainty. Therefore, the number of components of each vector R is n_{sim}, being $n_{sim} = q^{n_u}$ and n_u the number of uncertain variables.

$$R = \begin{pmatrix} R_1 \\ R_2 \\ \vdots \\ R_{n_{sim}} \end{pmatrix} \tag{14}$$

2. Then it loads the data vectors of the uncertain variable values that are input to the code, which in this case is only one V_1 containing n_q values. In general, we will have $n_u \times n_q$ data. For this case it simplifies to:

$$V_1 = \begin{pmatrix} V_{1_1} \\ V_{1_2} \\ \vdots \\ V_{1_{n_{sim}}} \end{pmatrix} \tag{15}$$

3. Because there is only one uncertain variable, then the calculation of the polynomial base is very simple and reduces when the PCE is truncated at order 4 to:

$$Base = \begin{pmatrix} H_0 = 1 \\ H_1 = 2x \\ H_2 = 4x^2 - 2 \\ H_3 = 8x^3 - 12x \\ H_4 = 16x^4 - 48x^2 + 12 \end{pmatrix} \tag{16}$$

4. There are five weights w_j and five roots x_j because we use Gaussian-Hermite quadrature of order 5 that make the calculation of the integrals of the quadrature by Gauss-Hermite procedure exact for integrations of polynomials up to order 9. The weights are:

$$w = \begin{pmatrix} w_1 = 0.019932 \\ w_2 = 0.393619 \\ w_3 = 0.945308 \\ w_4 = 0.393619 \\ w_5 = 0.019932 \end{pmatrix} \tag{17}$$

5. Calculation of the alpha coefficients α_n of the Polynomial Chaos Expansion.
   a. The objective is to calculate the alpha coefficients in the following way:

$$\alpha_n = \frac{\langle R\phi_n \rangle}{\langle {\phi_n}^2 \rangle} \tag{18}$$

   b. The first step is to calculate the denominator $\langle {\phi_n}^2 \rangle$. This result is direct and does not require values obtained from the simulations because ϕ_n are the Hermite polynomials.

$$\langle {\phi_n}^2 \rangle = \sigma^{2n}\, n! \tag{19}$$

   c. Next, we will calculate the numerator $\langle R\phi_n \rangle$. This is done by solving the integral using Gaussian-Hermite quadrature obtaining the equation explained in Appendix A.

$$\langle R\phi_n \rangle = \frac{\sigma^n}{\sqrt{\pi}\, 2^{n/2}} \sum_{j=1}^{5} w_j\, R\left(\mu + \sqrt{2}\,\sigma\, x_j\right) H_n\left(x_j\right) \tag{20}$$

6. Using the alpha coefficients α_n it is possible to obtain the mean and standard deviation values of each of the variables resulting from the R arrays.

$$\mu = \alpha_0 \tag{21}$$

$$\sigma^2 = \sum_{n=1}^{5} {\alpha_n}^2 \cdot \langle {\phi_n}^2 \rangle \tag{22}$$

5 RESULTS AND DISCUSSION

The first thing that was observed was the great dependence of the results on the turbulence model. Simulations of the open test showed that models based on the RANS equations tended to attenuate the velocities at the interface while those carried out using the LES turbulence model offered much higher accuracy (Figure 5). In addition, the results obtained for the GEMIX experiment revealed the possibility of using high-cost computational models (such as LES) for the CFD simulations if the uncertainty quantification is supported by an efficient method, such as the Polynomial Chaos by means of Gaussian quadrature.

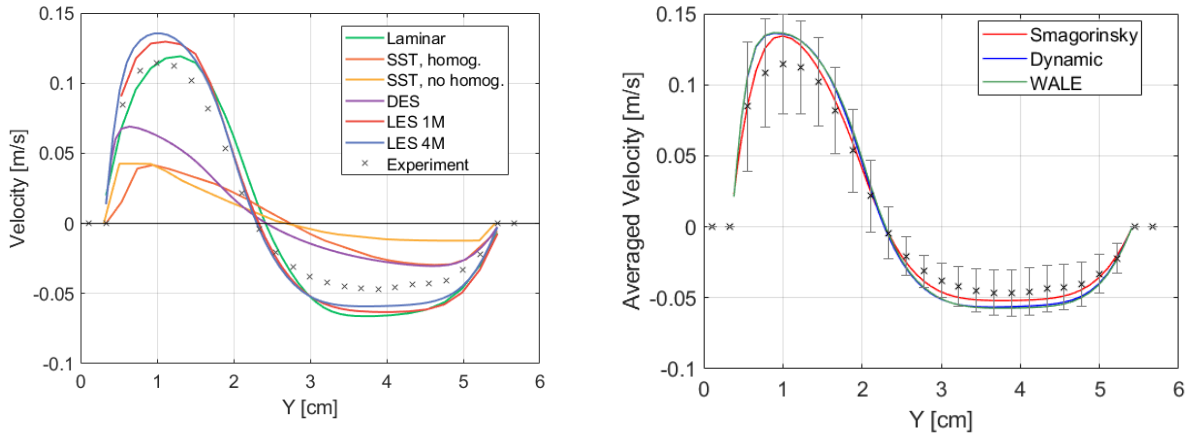

(a) (b)

Figure 5: *Cold-leg velocity comparison of the open test for different turbulence models (a) Laminar, SST, LES vs experiment, and (b) LES Smagorinsky, Dynamic and WALE vs experiment.*

Different models were tested removing transfer characteristics at the interface, modifying the surface tension, refining the mesh at the interface, etc. However, none of these modifications managed to avoid the disparity between results and experimental measurements of RANS-based models. Despite not having ample computational power, the LES turbulence model was essential for a correct performance of the simulation under these conditions (Figure 5a). The case of the DES turbulence model is decisive since it is located between the RANS and LES models. A clear improvement can be observed with respect to RANS, but the medium and small scales of turbulence are overestimated. This leads to the appearance of a much more diffuse interface in which the phases are mixed more than expected. In the research carried out by Hassan et al. (2021) a similar behavior is observed when $k-\omega$ SST (RANS model) is used in the simulations. However, the authors obtain much better results when using the RKE (Realizable $k-\epsilon$) or SKE (Standard $k-\epsilon$) turbulence models. The laminar model gives good results for the cold-leg. However, in the downcomer the motion is influenced by the turbulent mixing of both fluids so the use of a laminar model was discarded.

The resolution capability of the three LES models implemented in Ansys (Smagorinsky, WALE and Dynamic LES) was evaluated in the cold leg test section (see Section 2 for more information about the measurement zones). The results, as shown in the Figure 5b, are very close to each other, so it could be said that all three are valid for this simulation. The Euclidean distance (O'Neill, 2006) and the Mahalanobis distance (Mahalanobis, 1936) between experiment and each simulation were used as a method to estimate how close the results to the experimental measurements are. The model which results are closer for the velocities at the cold leg measurement zone was the Smagorinsky.

Finally, tests of the open test ended after the successful realization of the Polynomial Chaos by means of Gaussian quadrature for the quantification of the uncertainty. Figure 6 shows the comparison between the velocity obtained in the simulation and the experimental measurement for the cold leg and the downcomer. The shaded areas depicted in Figures 6 and 7 represent the

uncertainty band of the simulation results. Predicted velocities are quite close to the experimental measurements, although the simulation does not capture all the points. As mentioned previously, the LES turbulence model is very effective in this type of situation, but it requires a very fine mesh and a very small timestep. There are no data for the concentration in the open test, so this variable is studied only in the blind test.

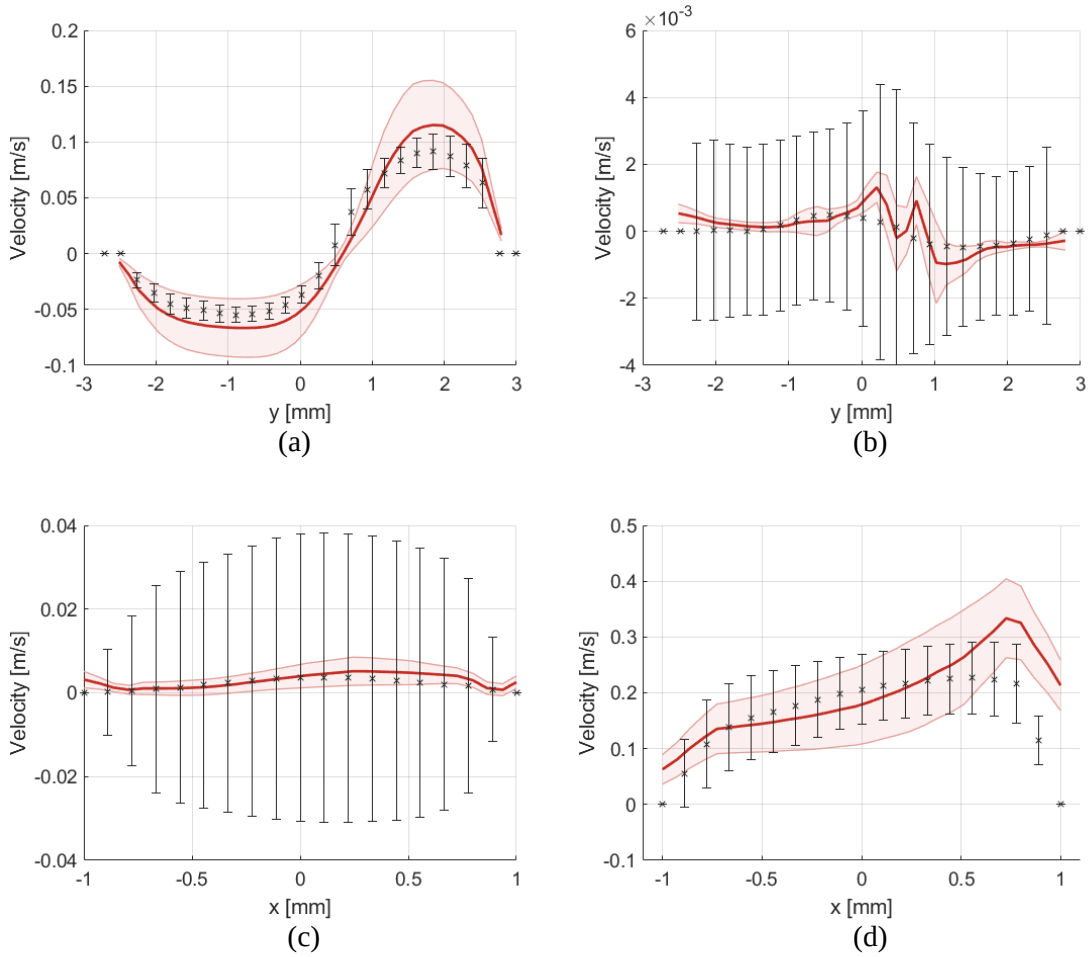

Figure 6: *Velocities of the open test obtained after the application of Polynomial Chaos Expansion by Gauss-Hermite quadrature. Experiment represented in black and the simulations in red. a) longitudinal velocity in the cold-leg, b) transversal velocity in the cold-leg, c) downward velocity in the downcomer and d) transversal velocity in the downcomer.*

As summary for the open test, the experimental measurements obtained by PIV in the TAMU installation are predicted quite well by Ansys CFX code. The domain of the fluid must be generated in such a way that the meshing does not have problems of cell quality. All those conflicting areas must either be treated carefully during the discretization or eliminated. The selected turbulence model has a great influence on the result obtained. RANS models are not capable of simulating the wavy interface of the cold-leg. The deviation between the simulations using these turbulence models and the experiment is amplified over time and tend to overestimate the mixing and turbulence between the two fluids. Turbulence models based on

Large Eddy Simulation can reproduce the behavior more accurately in exchange for a considerably higher computational cost. In the case of the UPV the cold-leg zone is predicted quite accurately as the motion is produced by gravity and buoyancy forces. For the downcomer, the turbulent mixing between the high-density current and the low-density current mainly influence the flow. This phenomenon is predicted with less accuracy, although the orders of magnitude are correctly maintained. The cell size therefore plays an important role in this zone improving the results as its value is reduced. At the WGAMA group, meeting in Paris in 2019 several organizations recognized the enormous difficulties they had encountered in predicting the vertical downward velocity of the mixture in the downcomer. The uncertainty analysis has been carried out by Polynomial Chaos Expansion and the results are satisfactory despite considering only the difference in density as an input uncertain variable.

For the blind test, a change in geometry and meshing was carried out to adjust the new liquid level of the high-density tank. To carry out the new uncertainty quantification, five new simulations by means of a 4 million cells mesh have been run.

The shape of the velocity profile is correct as shown in Figure 7 (a) and (b). However, the inflexion point, which is correctly predicted in the first time average (5-10s) is slightly shifted downwards for the following time intervals (10-15s) and (15-22s). The velocity of the low-density fluid is predicted accurately, but the high-density fluid is above the experimental measurements for the latest time averages. Similar behavior is observed by Lai et al. (2020) and Hassan et al. (2021) where the velocities difference between experiment and simulation increases over time.

There is an important scattering in the shape of the velocity profile in the downcomer, Figure 7 (c) and (d). In general, the jet of our simulations seems to be concentrated on the right side of the downcomer where its velocity is higher than on the left side. This behavior seems to be recurrent for those participants that have used RANS, URANS or LES with a low number of cells in the grid.

Figure 7 (e) and (f) shows that the vertical position of the stratification of concentrations (where concentrations change from low-density fluid to high-density fluid) is displaced downwards. This gap remains for the following intervals. For the initial time average (5-10s) the concentration values of the high-density fluid are below the experimental values, but they hit the experiment ones in the following intervals. This is probably due to the diffusion that appears at the interface or the possible offset of the high-density flow front in the measurement zone.

It should be noted that it is strange that fairly good inflexion points are obtained for the velocity profile (v = 0 m/s) but the concentration profile does not match in any of the cases. In general, for our case, it is observed that the deviations that occur in the concentration of the high-density fluid are recovered over time. This is indicative that our results are slightly shifted presumably due to the mesh resolution requirements of the LES model. Further research is needed to identify the problem. Looking at the velocities, the accuracy for the low-density fluid

is very good, but for the high-density fluid the values are above the experimental one. This situation seems to be recurrent in most of the participants and it should be studied in detail.

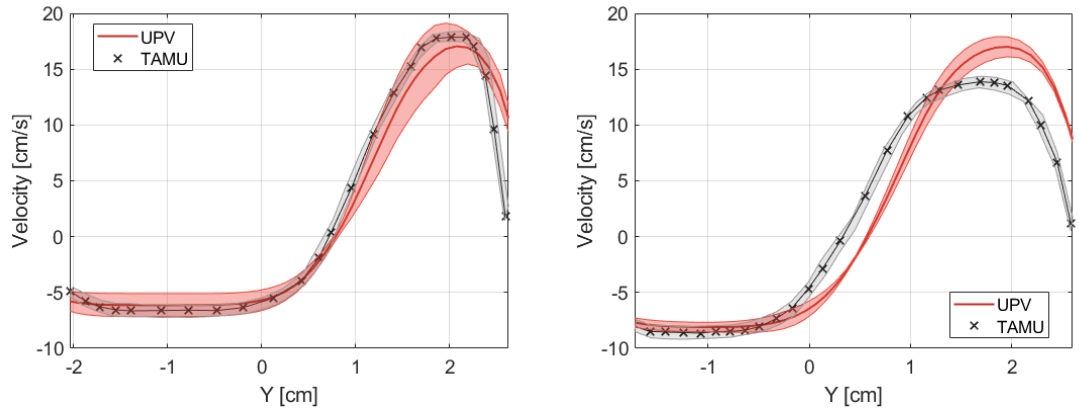

(a) Velocity CL 5-10s average

(b) Velocity CL 10-15s average

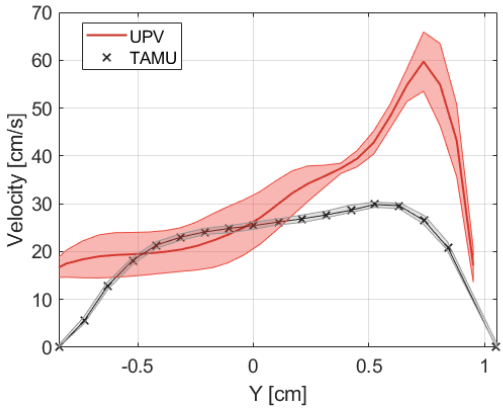

(c) Velocity DC 10.5-15.5s average

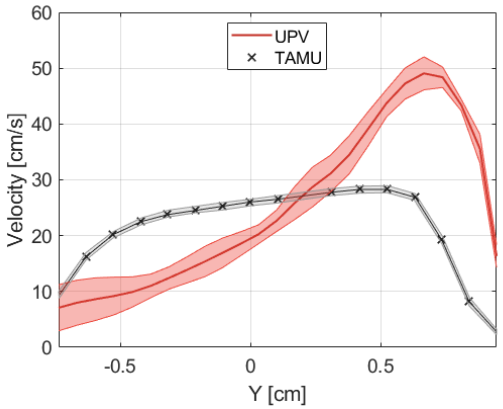

(d) Velocity DC 25.5-30.5s average

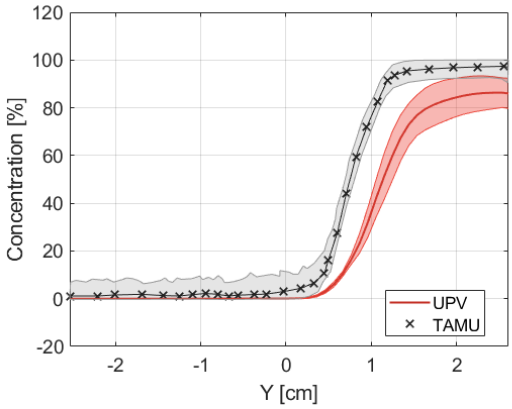

(e) Concentration CL 5-10s average

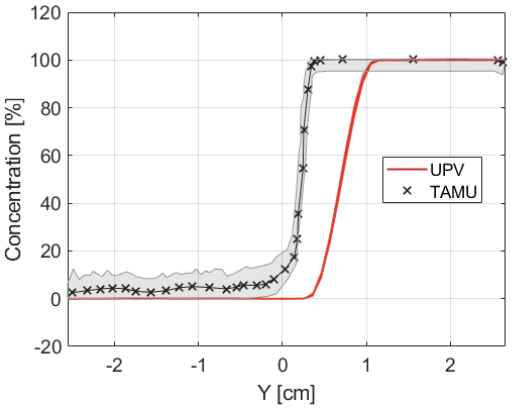

(f) Concentration CL 25.5-30.5s average

Figure 7: *Velocities of the blind test obtained after the application of Polynomial Chaos Expansion by Gauss Square. (a) longitudinal velocity in the cold-leg (CL) for the time average 5-10s, (b) longitudinal velocity in the cold-leg (CL) for the time average 10-15s, (c) downward velocity in the downcomer (DC) for the time average*

10.5-15.5s, (d) downward velocity in the downcomer (DC) for the time average 25.5-30.5s, (e) concentration in the cold-leg (CL) for the time average 5-10s and (f) concentration in the cold-leg (CL) for the time average 15-22.24s

6 CONCLUSIONS

The Institute for Energy Engineering of the Polytechnic University of Valencia has participated in the OECD Cold-Leg Mixing Benchmark by providing data from both the simulations and the uncertainty quantification. Our work is included within a project with the Spanish Nuclear Safety Council, aimed at seeking a set of good practices in the use of CFD codes to increase know-how in this field of knowledge.

Firstly, the most important characteristics of the experimental facility developed by Texas A&M University have been described. The properties of the fluids, the boundary conditions of the experiments and the measurements have been detailed. From the geometry provided by the developers of the experiment, a 4 million node mesh has been created using ICEM CFD and imported to Ansys CFX to generate the model. The turbulence model has been decisive for the accuracy of the results, so it was decided to use Large Eddy Simulations that filters the small scales of the turbulence and substitute them by an average effect. Other RANS based models tended to increase the mixing of the fluids resulting in a reduction of the velocities.

The steps followed to apply the Polynomial Chaos Expansion as a method of uncertainty quantification are explained and an appendix has been included with the procedure to ensure the orthogonality of the polynomials. The Gauss-Hermite Quadrature PCE is more efficient when the number of uncertain variables is small, so density was selected as the most relevant uncertain input variable. Therefore, selecting four as the order of the polynomial chaos expansion and five the quadrature order, the resulting number of simulations required was five. The uncertainty in the density difference between fluids follows a normal probability distribution thus Hermite polynomials were used.

For both the open and the blind test, the velocities obtained in the cold-leg are quite accurate, slightly overestimating the maximum value. However, in the downcomer the shape of the velocity profile is not correctly predicted, although, the order of magnitude is correct. In this area, simulation results show an increase in velocity on the inside of the downcomer which reduces its value as it approaches the outside. The profile of the concentrations is correct but there is a gap in the transition zone that is maintained for different time intervals. This difference leaves room for doubt because in the velocity profile this gap is not observed so further investigation is needed.

ACKNOWLEDGEMENTS

This work was supported by the project THAIS co-financed by the CSN (Nuclear Safety Council of Spain) and the UPV (Polytechnical University of Valencia). The authors would also

like to acknowledge the Texas A&M University for the experimental measurements, the OECD/NEA for organizing the benchmark and all the participants who make it possible.

REFERENCES

Abramovitz, M., Stegun, I.A., 1972. Handbook of Mathematical Functions with Formulas, Graphs and Mathematical Tables., National Bureau of Standards Applied Mathematics Series.

Andreani, M., Badillo, A., Kapulla, R., 2016. Synthesis of the OECD/NEA-PSI CFD benchmark exercise. Nucl. Eng. Des. 299, 59–80. https://doi.org/10.1016/j.nucengdes.2015.12.029

Askey, Richard., Wilson, J., 1985. Some basic hypergeometric orthogonal polynomials that generalize Jacobi polynomials. Mem. Am. Math. Soc. 54, 0–0. https://doi.org/10.1090/memo/0319

Askey, R., Wilson, J.A., 1985. Some basic hypergeometric orthogonal polynomials that generalize Jacobi polynomials. Am. Math. Soc. 319.

ASME V&V 20, 2009. Standard for Verification and Validation in Computational Fluid Dynamics and Heat Transfer ASME V & V 20-2009. Am. Soc. Mech. Eng. 102.

Badillo, A., Kapulla, R., Niceno, B., 2013. Uncertainty Quantification in CFD Simulations of Isokinetic Turbulent Mixing Layers, in: The 15th International Topical Meeting on Nuclear Reactor Thermal-Hydraulics, NURETH-15.

Canonsburg, T.D., 2011. ANSYS Meshing User ' s Guide. Knowl. Creat. Diffus. Util. 15317, 724–746.

Chang, S.K., Kim, S., Song, C.H., 2014. Turbulent mixing in a rod bundle with vaned spacer grids: OECD/NEA-KAERI CFD benchmark exercise test. Nucl. Eng. Des. 279, 19–36. https://doi.org/10.1016/j.nucengdes.2014.05.013

Crestaux, T., Le Maître, O., Martinez, J.M., 2009. Polynomial chaos expansion for sensitivity analysis. Reliab. Eng. Syst. Saf. 94, 1161–1172. https://doi.org/10.1016/j.ress.2008.10.008

D 'auria, F., Camargo, C., Mazzantini, O., 2012. The Best Estimate Plus Uncertainty (BEPU) approach in licensing of current nuclear reactors. Nucl. Eng. Des. 248, 317–328. https://doi.org/10.1016/j.nucengdes.2012.04.002

Fokken, J., Krohn, B., Kapulla, R., Niceno, B., Prasser, H.-M., Badillo, A., 2019. NEA Benchmark Exercise : Computational Fluid Dynamic Prediction and Uncertainty Quantification of a GEMIX Mixing Layer Test, NEA/CSNI/R(2017)19.

Hassan, M., Xiong, J., Cheng, X., 2021. Unsteady RANS simulation of OECD-TAMU cold-leg mixing benchmark. Nucl. Eng. Des. 372, 110978. https://doi.org/10.1016/j.nucengdes.2020.110978

Hessling, J.P., 2013. Deterministic Sampling for Propagating Model Covariance. Soc. Ind. Appl. Math. Am. Stat. Assoc. 1, 297–318. https://doi.org/https://doi.org/10.1137/120899133

Kim, J., 2019. Evaluation of RANS k – ε calculations for turbulent stably stratified layers based on GEMIX experiments using the CUPID code. Int. Commun. Heat Mass Transf. 108, 104341. https://doi.org/10.1016/j.icheatmasstransfer.2019.104341

Knio, O.M., Le Maître, O.P., 2006. Uncertainty propagation in CFD using polynomial chaos decomposition, Fluid Dynamics Research. https://doi.org/10.1016/j.fluiddyn.2005.12.003

Krpan, R., Končar, B., 2018. Simulation of Turbulent Wake at Mixing of Two Confined Horizontal Flows. Sci. Technol. Nucl. Install. 2018. https://doi.org/10.1155/2018/5240361

Lai, J.K., Merzari, E., Hassan, Y.A., Fischer, P., Marin, O., 2020. Verification and validation of large eddy simulation with Nek5000 for cold leg mixing benchmark. Nucl. Eng. Des. 358, 110427. https://doi.org/10.1016/j.nucengdes.2019.110427

Lucor, D., Meyers, J., Sagaut, P., 2007. Sensitivity analysis of large-eddy simulations to subgrid-scale-model parametric uncertainty using polynomial chaos. J. Fluid Mech. 585, 255–279. https://doi.org/10.1017/S0022112007006751

Mahaffy, J., Chung, B., Dubois, F., Ducros, F., Graffard, E., Heitsch, M., Henriksson, M., Komen, E., Moretti, F., Morii, T., Mühlbauer, P., Rohde, U., Scheuerer, M., Smith, B.L., Song, C., Watanabe, T., Zigh, G., 2014. Best Practice Guidelines for the Use of CFD in Nuclear Reactor Safety Applications, Nea/Csni/R(2014)11.

Mahalanobis, P.C., 1936. On The Generalized Distance in Statistics, Proceedings of the National Institute of Sciences of India.

Muñoz-Cobo, J.L., Miquel, A., Escrivá, A., Berna, C., Rivera, Y., 2018. Efficient uncertainty quantification in nuclear thermal-hydraulic simulations by means of polynomial chaos expansion., in: ANS Best Estimate Plus Uncertainty International Conference (BEPU 2018) Real Collegio, Lucca, Italy, May 13-19, 2018. p. 11.

Najm, H.N., 2009. Uncertainty Quantification and Polynomial Chaos Techniques in Computational Fluid Dynamics. Annu. Rev. Fluid Mech. 41, 35–52. https://doi.org/https://doi.org/10.1146/annurev.fluid.010908.165248

O'Neill, B., 2006. Calculus on Euclidean Space, in: Elementary Differential Geometry. Elsevier, pp. 3–42. https://doi.org/10.1016/b978-0-12-088735-4.50005-5

OECD/NEA/CSNI, 2016. The Nuclear Energy Agency–Paul Scherrer Institut Computation Fluid Dynamics Benchmark Exercise, Nea/Csni/R(2016)2.

OECD/NEA/CSNI, Smith, B.L., Mahaffy, J.H., Angele, K., Westin, J., 2011. Report of the OECD/NEA-Vattenfall T-Junction Benchmark exercise.

Orea, D., Vaghetto, R., Nguyen, T., Hassan, Y., 2020. Experimental measurements of flow mixing in cold leg of a pressurized water reactor. Ann. Nucl. Energy 140, 107137. https://doi.org/10.1016/j.anucene.2019.107137

Prošek, A., Končar, B., Leskovar, M., 2017. Uncertainty analysis of CFD benchmark case using optimal statistical estimator. Nucl. Eng. Des. 321, 132–143. https://doi.org/10.1016/j.nucengdes.2016.12.008

Rakhimov, A.C., Visser, D.C., Komen, E.M.J., 2019. Uncertainty Quantification method for CFD applied to the turbulent mixing of two water layers – II: Deterministic Sampling for input uncertainty. Nucl. Eng. Des. 348, 146–158. https://doi.org/10.1016/j.nucengdes.2019.04.016

Rakhimov, A.C., Visser, D.C., Komen, E.M.J., 2018. Uncertainty Quantification method for CFD applied to the turbulent mixing of two water layers. Nucl. Eng. Des. 333, 1–15. https://doi.org/10.1016/j.nucengdes.2018.04.004

Salvetti, M. V., Meldi, M., Bruno, L., Sagaut, P., 2018. Reliability of large-eddy simulations: Benchmarking and uncertainty quantification. ERCOFTAC Ser. 24, 15–23. https://doi.org/10.1007/978-3-319-63212-4_2

Simoneau, J.-P., Champigny, J., Gelineau, O., 2010. Applications of large eddy simulations in nuclear field. Nucl. Eng. Des. 240, 429–439. https://doi.org/10.1016/j.nucengdes.2008.08.018

Smith, B.L. (PSI), Bieder, U. (CEA), Grafard, E. (IRSN), Heitsch, M. (GRS), Henriksson, M. (Vattenfall), Höhne, T. (FZD), Komen, E. (NRG), Mahaffy, J. (PSU), Moretti, F. (UPisa), Morii, T. (JNES), Mühlbauer, P. (NRI), Rohde, U. (FZD), Scheuerer, M. (GRS), Song, C.-H. (KAERI), Zigh, G. (USNRC), 2008. Assessment of Computational Fluid Dynamics (CFD) for Nuclear Reactor Safety Problems, NEA/CSNI/R(2007)13.

Smith, B. L., Mahaffy, J.H., Angele, K., 2013. A CFD benchmarking exercise based on flow mixing in a T-junction. Nucl. Eng. Des. 264, 80–88. https://doi.org/10.1016/j.nucengdes.2013.02.030

Smith, B.L., Song, C.H., Chang, S.K., Lee, J.R., Kim, J.W., 2013. Report of the OECD/NEA KAERI Rod Bundle CFD Benchmark Exercise.

Wiener, N., 1938. The homogeneous chaos. Am. J. Math. 60(4), 897–936.

Xiu, D., Karniadakis, G.E., 2003a. Modeling uncertainty in flow simulations via generalized polynomial chaos. J. Comput. Phys. 187, 137–167. https://doi.org/10.1016/S0021-9991(03)00092-5

Xiu, D., Karniadakis, G.E., 2003b. Modeling uncertainty in flow simulations via generalized polynomial chaos. J. Comput. Phys. 187, 137–167. https://doi.org/10.1016/S0021-9991(03)00092-5

APPENDIX A. ORTHOGONALITY OF HERMITE POLYNOMIALS TO APPLY POLYNOMIAL CHAOS EXPANSION WITH AN UNCERTAIN VARIABLE OF ANY MEAN AND VARIANCE

This appendix addresses the issue of Hermite polynomials orthogonality when it is necessary to perform a variable change. To apply the Polynomial Chaos Expansion in the case of an uncertain variable with Gaussian distribution function it is necessary to use Hermite polynomials. However, it is most likely that our uncertain variable will have a mean and variance different from 0 and 1. Therefore, it is necessary to obtain Hermite polynomials that are orthogonal to the new variable characteristics.

It is easy to find in the literature the Hermite polynomials that satisfy the following relation:

$$\langle H_n^2 \rangle = \int_{-\infty}^{\infty} e^{-x^2} \, H_n^2(x) \, dx = h_n = \sqrt{\pi} \, 2^n \, n! \tag{A1}$$

Note that the polynomials H_n are orthogonal on $(-\infty, \infty)$ for the weight function $w(x) = e^{-x^2}$. Hermite polynomials can also be found as He_n, but the relationship is similar as shown in eq. A2.

$$\langle He_n^2 \rangle = \int_{-\infty}^{\infty} e^{-\frac{x^2}{2}} \, He_n^2(x) \, dx = \sqrt{2\pi} \, n! \tag{A2}$$

Some authors move the constant $\sqrt{2\pi}$ into the integral so the expression can be arranged according to the eq. A2.

$$\langle He_n^2 \rangle = \int_{-\infty}^{\infty} p(x)\, He_n^2(x)\, dx = \int_{-\infty}^{\infty} \frac{1}{\sqrt{2\pi}} e^{-\frac{x^2}{2}}\, He_n^2(x)\, dx = \ n! \tag{A3}$$

Being $p(x)$ the probability density function for a normal distribution with $\mu = 0$ and $\sigma = 1$. The relation between both H_n and He_n correspond to the equations A4 and A5.

$$H_n(x) = 2^{n/2}\, He_n\left(\sqrt{2}x\right) \tag{A4}$$

$$He_n(x) = 2^{-(n/2)}\, H_n\left(\frac{x}{\sqrt{2}}\right) \tag{A5}$$

Then, the same reasoning is followed, but starting from the probability density function shown in eq. A6 and then calculating the orthogonal Hermite polynomials.

$$p(x) = \frac{1}{\sqrt{2\pi}\sigma} e^{-\frac{x^2}{2\sigma^2}} \tag{A6}$$

$$\langle \left(He_n^{\sigma^2}\right)^2 \rangle = \int_{-\infty}^{\infty} p(x)\, \left(He_n^{\sigma^2}(x)\right)^2\, dx = \int_{-\infty}^{\infty} \frac{1}{\sqrt{2\pi}\sigma} e^{-\frac{x^2}{2\sigma^2}}\, \left(He_n^{\sigma^2}(x)\right)^2\, dx \tag{A7}$$

For this scenario the new polynomials are denoted as $He_n^{\sigma^2}$ and the relation with H_n and He_n is the next one.

$$He_n^{\sigma^2}(x) = \sigma^n\, He_n\left(\frac{x}{\sigma}\right) = \frac{\sigma^n}{2^{n/2}} H_n\left(\frac{x}{\sqrt{2}\sigma}\right) \tag{A8}$$

Then, it is possible to follow the reasoning started in eq. A7:

$$\begin{aligned} \langle \left(He_n^{\sigma^2}\right)^2 \rangle &= \int_{-\infty}^{\infty} \frac{1}{\sqrt{2\pi}\sigma} e^{-\frac{x^2}{2\sigma^2}}\, \left(He_n^{\sigma^2}(x)\right)^2\, dx \\ &= \left(\frac{\sigma^2}{2}\right)^n \int_{-\infty}^{\infty} \frac{1}{\sqrt{2\pi}\sigma} e^{-\frac{x^2}{2\sigma^2}} \left(H_n\left(\frac{x}{\sqrt{2}\sigma}\right)\right)^2\, dx \end{aligned} \tag{A9}$$

Finally, applying the variable change $t = \frac{x}{\sqrt{2}\sigma}$ and $dt = \frac{dx}{\sqrt{2}\sigma}$.

$$\langle \left(He_n^{\sigma^2}\right)^2 \rangle = \left(\frac{\sigma^2}{2}\right)^n \frac{1}{\sqrt{\pi}} \int_{-\infty}^{\infty} e^{-t^2}\, {H_n}^2(t)\, dt \tag{A10}$$

The result for $\frac{1}{\sqrt{\pi}} \int_{-\infty}^{\infty} e^{-t^2}\, {H_n}^2(t)\, dt$ is given by eq. A1, so the result for the new Hermite polynomials $\langle \left(He_n^{\sigma^2}\right)^2 \rangle$ is also known.

$$\langle \left(He_n^{\sigma^2}\right)^2 \rangle = \left(\frac{\sigma^2}{2}\right)^n \frac{1}{\sqrt{\pi}} \sqrt{\pi}\, 2^n\, n! = \sigma^{2n}\, n! \tag{A11}$$

There is one more step needed before obtaining the last expression for the calculation of the Polynomial Chaos Expansion. As a quick reminder, our simulations will be performed after changing the variable. Following the relation $x^{in} = \mu + \sqrt{2}\, \sigma\, t$ it is possible to obtain the input values that we will have to introduce in our code. Then, it is necessary to repeat the process for the probability density function of eq. A12.

$$p(x) = \frac{1}{\sqrt{2\pi}\sigma} e^{-\left(\frac{x-\mu}{\sqrt{2}\,\sigma}\right)^2} \tag{A12}$$

After performing an intermediate variable change $x = t - \mu$ and $dt = dx$ and starting from the eq. A8

$$He_n^{\sigma^2}(t-\mu) = \frac{\sigma^n}{2^{n/2}} H_n\left(\frac{t-\mu}{\sqrt{2}\,\sigma}\right) \tag{A13}$$

Therefore the new orthogonal polynomials are defined as follows:

$$He_n^{(\sigma^2,\mu)}(x) = \frac{\sigma^n}{2^{n/2}} H_n\left(\frac{x-\mu}{\sqrt{2}\,\sigma}\right) \tag{A14}$$

Then,

$$\langle\left(He_n^{(\sigma^2,\mu)}\right)^2\rangle = \langle{\phi_n}^2\rangle = \int_{-\infty}^{\infty} \frac{1}{\sqrt{2\pi}\sigma} e^{-\left(\frac{x-\mu}{\sqrt{2}\,\sigma}\right)^2} \left(He_n^{(\sigma^2,\mu)}(x)\right)^2 dx = \sigma^{2n}\, n! \tag{A15}$$

The definition of $He_n^{(\sigma^2,\mu)}$ is shown in eq. A14, his module $\langle\left(He_n^{(\sigma^2,\mu)}\right)^2\rangle$ in eq. A15 so the only missing term to calculate the alpha coefficients $\alpha = \frac{\langle R\phi_n\rangle}{{\phi_n}^2}$ of the Polynomial Chaos Expansion by Gauss-Quadrature is displayed in eq. A16.

$$\langle R\phi_n\rangle = \int_{-\infty}^{\infty} \frac{1}{\sqrt{2\pi}\sigma} e^{-\left(\frac{x-\mu}{\sqrt{2}\,\sigma}\right)^2} R(x)\, He_n^{(\sigma^2,\mu)}(x)\, dx \tag{A16}$$

The last variable change is $x^{in} = \mu + \sqrt{2}\,\sigma\, t$ and $dx^{in} = dt\,\sqrt{2}\,\sigma$. Note that we have included the superscript in referring to the fact that this variable x corresponds to the uncertain variable of our simulation input.

$$\langle R\phi_n\rangle = \frac{1}{\sqrt{\pi}} \int_{-\infty}^{\infty} e^{-t^2} R\left(\mu + \sqrt{2}\,\sigma\, t\right) He_n^{(\sigma^2,\mu)}\left(\mu + \sqrt{2}\,\sigma\, t\right) dt \tag{A17}$$

Substituting orthogonal polynomials $He_n^{\sigma^2\mu}$ by eq. A14.

$$\begin{aligned}\langle R\phi_n\rangle &= \frac{1}{\sqrt{\pi}} \int_{-\infty}^{\infty} e^{-t^2}\, R\left(\mu + \sqrt{2}\,\sigma\, t\right) \frac{\sigma^n}{2^{n/2}}\, H_n\left(\frac{\mu + \sqrt{2}\,\sigma\, t - \mu}{\sqrt{2}\,\sigma}\right) dt \\ &= \frac{\sigma^n}{\sqrt{\pi}\, 2^{n/2}} \int_{-\infty}^{\infty} e^{-t^2}\, R\left(\mu + \sqrt{2}\,\sigma\, t\right)\, H_n(t)\, dt\end{aligned} \tag{A18}$$

Finally, as it has been exposed in this article, the integral has been solved by means of Gauss quadrature following the eq. A19.

$$\langle R\phi_n\rangle = \frac{\sigma^n}{\sqrt{\pi}\, 2^{n/2}} \sum_{j=1}^{5} w_j\, R\left(\mu + \sqrt{2}\,\sigma\, t_j\right) H_n\left(t_j\right) \tag{A19}$$